Bending control and stability of functionally graded dielectric elastomers

Yipin Su[1,2,3], Ray W. Ogden[4], Michel Destrade[1,2]

[1] School of Mathematics, Statistics and Applied Mathematics
NUI Galway, University Road, Galway, Ireland

[2] Department of Engineering Mechanics, Zhejiang University
Hangzhou 310027, PR China

[3] Sonny Astani Department of Civil and Environmental Engineering
University of Southern California, Los Angeles, CA 90089, USA

[4] School of Mathematics and Statistics, University of Glasgow
University Place, Glasgow G12 8SQ, UK

Abstract

A rectangular plate of dielectric elastomer exhibiting gradients of material properties through its thickness will deform *inhomogeneously* when a potential difference is applied to compliant electrodes on its major surfaces, because each plane parallel to the major surfaces will expand or contract to a different extent. Here we study the voltage-induced bending response of a functionally graded dielectric plate on the basis of the nonlinear theory of electroelasticity, when both the elastic shear modulus and the electric permittivity change with the thickness coordinate. The theory is illustrated for a neo-Hookean electroelastic energy function with the shear modulus and permittivity varying linearly across the thickness. In general the bending angle increases with the potential difference, and this enables the material inhomogeneity to be tuned to control the bending shape. We derive the Hessian criterion that ensures stability of the bent configurations in respect of a general form of electroelastic constitutive law specialized for the considered geometry. This requires that the Hessian remains positive. For the considered model we show that the bent configuration is stable until the voltage reaches the value for which the cross section of the bent configuration forms a complete circle.

Key words: Large bending; functionally graded dielectric elastomer; nonlinear electroelasticity; electroelastic stability.

1 Introduction

Dielectric elastomers are soft active materials capable of undergoing large deformations rapidly in response to an applied potential difference (voltage) across their thickness, and have therefore attracted considerable academic and industrial attention in recent years [1–5]. *Shape control*, which is eagerly pursued in dielectric elastomers, has considerable potential for applications to, for example, soft robots, energy harvest systems, actuators and sensors [6, 7]. Hence, based on the concept of *smart-bending actuation* [9, 14], an intelligent self-controlled switch can be designed to keep the working voltage in a desired range: as the voltage rises or falls, the material bends toward or away from a contact point so as to moderate the voltage automatically.

One clever strategy for designing voltage-responsive bending solids is to use dielectric elastomers with physical properties that vary in the thickness direction. When subject to a voltage through the thickness, a non-uniform deformation is generated in the material, which can result in a global bending. Dielectric-based multilayers composed of pre-stretched dielectric and inactive elastic layers have been proposed to realise shape control by tuning the applied voltage only, without any mechanical input [9, 14]. However, discontinuous shear stresses may arise at the interface of the layers, which may result in slide, exfoliation or crack formation during the bending deformation [9–11].

To overcome this potential problem, this paper proposes to study functionally graded dielectric elastomers (FGDEs) with material properties varying *continuously* through the thickness. Experimentally, bulk functionally graded materials (FGMs) can be manufactured by methods such as Powder Metallurgy Technique, Centrifugal Casting and Solid Freeform Technology [12], etc. To produce thin FGMs, techniques such as Physical or Chemical Vapour Deposition (PVD/C-VD), Plasma Spraying and Self-propagating High-temperature Synthesis (SHS) are more appropriate [13]. Spatial inhomogeneous dielectric properties can be introduced by embedding electroactive particles into a polymer FGM matrix unevenly through a well-established additive manufacturing (3D printing) process [14]. The electric field can be generated by applying a voltage through the flexible electrodes covered on the upper and lower faces of the resulting elastomers.

If the gradients of properties vary in a monotone manner though the plate thickness, we expect the expansion or contraction of each plane in the plate to also vary in the same way; hence, *the plate will bend*. Here we use the framework of nonlinear electroelasticity [15, 16] to investigate the nonlinear bending behaviour and the stability of such plates.

For an FGDE plate the required analysis, summarised in Section 2, is complicated by the inherent inhomogeneity, but we nonetheless manage to derive analytical formulas governing the voltage-induced bending of a plate made of a neo-Hookean dielectric with linear gradients in its material properties. In Section 3 we obtain numerical results showing the bent shape of the plate and the associated stress distributions. The results vary significantly with the selected values of the grading parameters.

For a plate with uniform properties, the onset of *pull-in instability* has been examined extensively, see for example the papers by Zhao and Suo [17], Lu et al. [18], Zhao and Wang [19], Zurlo et al. [20], or Su et al. [21, 22]. In general, the pull-in instability leads to

a dramatic thinning of the plate, thus triggering a giant deformation in the material. Here the corresponding phenomenon would be a sudden increase in the bending angle and, in general, a sudden thinning of the bent plate. However, we find (at least for the geometrical and material parameters chosen as examples) that this type of pull-in instability does not arise, because the maximal configuration of a closed circular ring is reached before the maximum in the voltage-stretch relation.

In Section 4, we examine the stability of the bent configuration on the basis of the positive definiteness of the second variation of the free energy. In particular, we derive the associated Hessian criterion in respect of a general form of free energy for the considered geometry. On this basis we find that the considered bent configurations are stable for the full range of the applied voltage up to the point where the in-plane section of the plate forms a complete circle, the upper limit of the voltage being dependent on the values of the grading parameters. These results, which we summarise in Section 5, have potential for informing the design of high-performance actuators and sensors.

2 Bending response of an FGDE plate

2.1 Kinematics and electric field

Consider an FGDE plate of initial length L, thickness A and width H, the latter being assumed to be much longer than its thickness and length. The solid occupies the region $0 \leq X_1 \leq A$, $-L/2 \leq X_2 \leq L/2$, $0 \leq X_3 \leq H$ in the reference configuration, and the faces $X_1 = 0, A$ are coated with flexible electrodes as depicted in Figure 1(a). The material properties are taken to be inhomogeneous with grading dependent on the thickness coordinate X_1.

On application of a potential difference V (voltage) across the electrodes the plate is bent into the shape shown in Figure 1(b), and the resulting deformation is assumed to have a plane strain character in the (X_1, X_2) plane, as in [9, 14]. In Figure 1(a) we have indicated the dependence on X_1 of the shear modulus μ and permittivity ε, which will be specified in Section 2.2. The material is assumed to be incompressible.

The deformation of the plate is described by the equations

$$r = \sqrt{r_a^2 + (r_b^2 - r_a^2)\frac{X_1}{A}}, \qquad \theta = \frac{2A}{r_b^2 - r_a^2}X_2, \qquad z = X_3, \qquad (2.1)$$

as in [23, 24], where (r, θ, z) are the cylindrical polar coordinates in the deformed configuration, and r_a, r_b are the radii of the inner and outer bent surfaces, respectively. The associated deformation gradient, denoted $\mathbf{F}$, has the diagonal form $\mathrm{diag}(\lambda^{-1}, \lambda, 1)$ with respect to the cylindrical polar axes, where

$$\lambda = \frac{2Ar}{r_b^2 - r_a^2} \qquad (2.2)$$

3

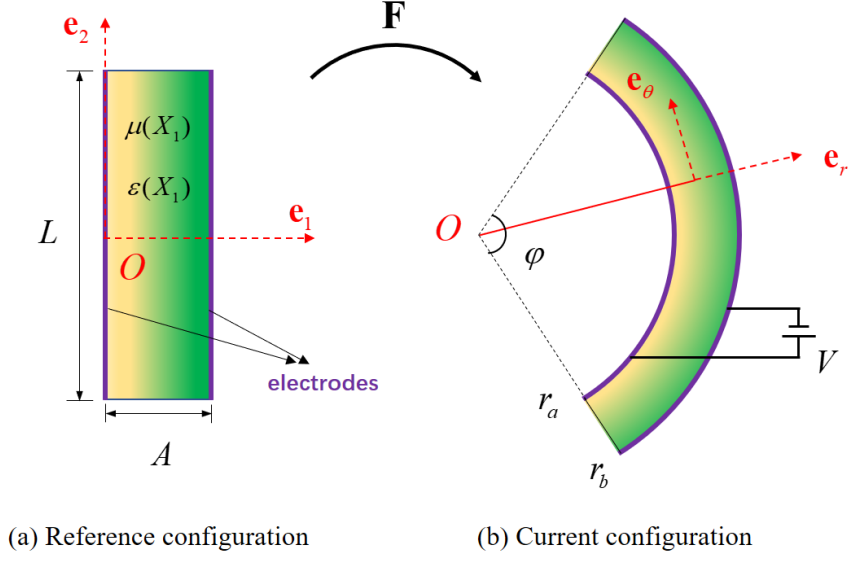(a) Reference configuration   (b) Current configuration

Figure 1: A block of FGDE with continuously varying shear modulus $\mu(X_1)$ and permittivity $\varepsilon(X_1)$ through the thickness, coated with two compliant electrodes. The layer bends when loaded with a voltage V across the electrodes, with the bending angle φ.

is the *circumferential stretch*. It takes the values

$$\lambda_a = \frac{2Ar_a}{r_b^2 - r_a^2}, \qquad \lambda_b = \frac{2Ar_b}{r_b^2 - r_a^2}, \tag{2.3}$$

on the inner and outer bent faces, respectively. It follows that the dependence of λ on X_1 is given by

$$\lambda^2 = \lambda_a^2 + (\lambda_b^2 - \lambda_a^2)\frac{X_1}{A}. \tag{2.4}$$

Note that, by taking $X_2 = L/2$ and $\theta = \varphi/2$ in $(2.1)_2$, we obtain an expression for the *bending angle* φ, namely

$$\varphi = (\lambda_b^2 - \lambda_a^2)L/(2A), \tag{2.5}$$

as given in [24]. Hence $\lambda = \varphi r/L$.

On application of the voltage V a radial electric field component, denoted E, is generated in the bent configuration of the material, assuming that edge effects can be neglected, and the corresponding electric displacement field component is denoted D. Each of E and D depends on r and is independent of θ and z. Maxwell's equation div $\mathbf{D} = 0$ then reduces to $\mathrm{d}(rD)/\mathrm{d}r = 0$, so that rD is constant. The corresponding Lagrangian field, given by $\mathbf{D}_\mathrm{L} = \mathbf{F}^{-1}\mathbf{D}$ in general for an incompressible material, reduces to the single component $D_\mathrm{L} = \lambda D$, which by (2.2) is therefore a *constant*.

4

2.2 Constitutive law

For an isotropic electroelastic material in general we take the energy to be a function of $\mathbf{F}$ and $\mathbf{D}_L$, but for the considered geometry, deformation and electric field, this reduces to dependence on λ and D_L. We denote the energy function by $\omega^*(\lambda, D_L)$.

The relevant components of the total Cauchy stress tensor are the radial and circumferential components, denoted τ_{rr} and $\tau_{\theta\theta}$, respectively. These satisfy the equilibrium equation

$$\frac{\mathrm{d}}{\mathrm{d}r}(r\tau_{rr}) = \tau_{\theta\theta}. \tag{2.6}$$

The stress difference $\tau_{\theta\theta} - \tau_{rr}$ and Lagrangian electric field $E_L = \lambda^{-1}E$ are obtained from the formulas

$$\tau_{\theta\theta} - \tau_{rr} = \lambda\frac{\partial\omega^*}{\partial\lambda}, \qquad E_L = \frac{\partial\omega^*}{\partial D_L}; \tag{2.7}$$

see, for example, [15, 16].

Since, from (2.2), λ is proportional to r, while D_L is constant, the combination of (2.6) and $(2.7)_1$ followed by integration, leads to

$$\tau_{rr} = \omega^* + K, \qquad \tau_{\theta\theta} = \lambda\frac{\partial\omega^*}{\partial\lambda} + \omega^* + K, \tag{2.8}$$

as derived in [24], where K is a constant to be determined from the boundary conditions, in a similar way to the situation in the purely elastic case [23].

Here we assume that the inner and outer surfaces of the bent sector at r_a and r_b are free of mechanical traction, so that

$$\tau_{rr}(r_a) = 0, \qquad \tau_{rr}(r_b) = 0, \tag{2.9}$$

there being no Maxwell stress on these surfaces.

For definiteness, we consider an energy function which has the form

$$\omega^*(\lambda, D_L) = W(\lambda) + \frac{D_L^2}{2\varepsilon\lambda^2}, \tag{2.10}$$

where W is derived from any isotropic purely elastic strain-energy function and we recall that $D = \lambda^{-1}D_L$.

The boundary conditions (2.9) provide two expressions for K,

$$-K = W(\lambda_a) + \frac{D_L^2}{2\varepsilon_a\lambda_a^2} = W(\lambda_b) + \frac{D_L^2}{2\varepsilon_b\lambda_b^2}, \tag{2.11}$$

and hence an expression for D_L^2, namely

$$D_L^2 = 2\varepsilon_a\varepsilon_b\lambda_a^2\lambda_b^2\frac{W(\lambda_b) - W(\lambda_a)}{\varepsilon_b\lambda_b^2 - \varepsilon_a\lambda_a^2}, \tag{2.12}$$

where ε_a and ε_b are the values of ε at $r = r_a$ and $r = r_b$, respectively, i.e. for $X_1 = 0, A$. The form of the function $\varepsilon(X_1)$ will be exemplified below. It follows that

$$K = -\frac{\varepsilon_b \lambda_b^2 W(\lambda_b) - \varepsilon_a \lambda_a^2 W(\lambda_a)}{\varepsilon_b \lambda_b^2 - \varepsilon_a \lambda_a^2}. \tag{2.13}$$

Let $\phi(X_1)$ denote the electrostatic potential through the thickness. Then, from Maxwell's equation $\mathrm{Curl}\,\mathbf{E}_{\mathrm{L}} = \mathbf{0}$ we have $\mathbf{E}_{\mathrm{L}} = -\mathrm{Grad}\,\phi$, which specializes here to $E_{\mathrm{L}} = -\mathrm{d}\phi/\mathrm{d}X_1$. The potential difference $\phi(0) - \phi(X_1)$ is the voltage V, which, on use of $(2.7)_2$ is given by

$$V = \int_0^A E_{\mathrm{L}}\mathrm{d}X_1 = \frac{2A}{\lambda_b^2 - \lambda_a^2} \int_{\lambda_a}^{\lambda_b} \lambda \frac{\partial \omega^*}{\partial D_{\mathrm{L}}}\mathrm{d}\lambda, \tag{2.14}$$

the latter change of variable making use of (2.4). For the model (2.10), this yields

$$V = \frac{2AD_{\mathrm{L}}}{\lambda_b^2 - \lambda_a^2} \int_{\lambda_a}^{\lambda_b} \frac{\mathrm{d}\lambda}{\lambda \varepsilon}, \tag{2.15}$$

and we recall that ε depends on X_1 and hence on λ.

To complete the formulation of the problem, we first note that the resultant force on the lateral end faces at $\theta = \pm\varphi/2$ vanishes since, with the help of the boundary conditions (2.9) and equation (2.6), it follows that

$$\int_{\lambda_a}^{\lambda_b} \tau_{\theta\theta}\mathrm{d}r = 0 \tag{2.16}$$

is automatically satisfied [24]. We then assume that there is no resultant moment on these faces so that *the block is bent by the application of a voltage alone.* This requires

$$\int_{r_a}^{r_b} r\tau_{\theta\theta}\mathrm{d}r = 0, \quad \text{equivalently} \quad \int_{\lambda_a}^{\lambda_b} \lambda\tau_{\theta\theta}\mathrm{d}\lambda = 0, \tag{2.17}$$

which, from $(2.8)_2$, yields

$$\int_{\lambda_a}^{\lambda_b} \lambda \left(\lambda \frac{\partial \omega^*}{\partial \lambda} + \omega^* + K \right) \mathrm{d}\lambda = 0, \tag{2.18}$$

and for the model (2.10),

$$\int_{\lambda_a}^{\lambda_b} \lambda(\lambda W_\lambda + W)\mathrm{d}\lambda - \frac{1}{2}D_{\mathrm{L}}^2 \int_{\lambda_a}^{\lambda_b} \left(\frac{1}{\lambda\varepsilon} + \frac{\varepsilon_\lambda}{\varepsilon^2} \right)\mathrm{d}\lambda + \frac{1}{2}K(\lambda_b^2 - \lambda_a^2) = 0, \tag{2.19}$$

where the subscript λ signifies the derivative with respect to λ.

Equations (2.12) and (2.13), respectively, give D_{L} and K in terms of λ_a and λ_b. Equation (2.15) then determines V also in terms of λ_a and λ_b, which we write in the form

$$V = f(\lambda_a, \lambda_b). \tag{2.20}$$

6

Once the form of W is prescribed, equation (2.19), after substituting for D_{L} and K, yields an implicit connection between λ_a and λ_b, which we write as

$$g(\lambda_a, \lambda_b) = 0. \tag{2.21}$$

Then, in principle, V can be determined in terms of λ_a (or λ_b).

For further specialization we now take W to be the *neo-Hookean strain-energy function*, which, for the considered plane deformation, has the form

$$W(\lambda) = \frac{\mu}{2}(\lambda^2 + \lambda^{-2} - 2), \tag{2.22}$$

where the shear modulus μ is functionally graded through the thickness, i.e. is a function of X_1.

Then the formulas (2.12) and (2.13) specialize to

$$D_{\mathrm{L}}^2 = \varepsilon_a \varepsilon_b \frac{\mu_b \lambda_a^2 (\lambda_b^2 - 1)^2 - \mu_a \lambda_b^2 (\lambda_a^2 - 1)^2}{\varepsilon_b \lambda_b^2 - \varepsilon_a \lambda_a^2}, \tag{2.23}$$

$$K = -\frac{1}{2} \frac{\mu_b \varepsilon_b (\lambda_b^2 - 1)^2 - \mu_a \varepsilon_a (\lambda_a^2 - 1)^2}{\varepsilon_b \lambda_b^2 - \varepsilon_a \lambda_a^2}, \tag{2.24}$$

where μ_a and μ_b are the values of $\mu(X_1)$ at $X_1 = 0, A$ $(r = r_a, r_b)$, and (2.19) becomes

$$\int_{\lambda_a}^{\lambda_b} \mu(3\lambda^3 - \lambda^{-1} - 2\lambda)\mathrm{d}\lambda - D_{\mathrm{L}}^2 \int_{\lambda_a}^{\lambda_b} \left(\frac{1}{\lambda\varepsilon} + \frac{\varepsilon_\lambda}{\varepsilon^2}\right)\mathrm{d}\lambda + K(\lambda_b^2 - \lambda_a^2) = 0. \tag{2.25}$$

To take this further we need to specify how μ and ε depend on X_1, and through the connection (2.4), on λ. We assume a simple *linear dependence* of μ and ε on X_1, as in [25, 26], here specified by

$$\mu(X_1) = \mu_a\left(1 - \alpha_\mu X_1/A\right), \qquad \varepsilon(X_1) = \varepsilon_a\left(1 + \alpha_\varepsilon X_1/A\right), \tag{2.26}$$

with $\mu_b = \mu_a(1 - \alpha_\mu)$ and $\varepsilon_b = \varepsilon_a(1 + \alpha_\varepsilon)$, where α_μ and α_ε are two dimensionless constants characterizing the functionally graded properties of the shear modulus and permittivity, respectively, of the material. The expressions for D_{L}^2 and K in (2.23) and (2.24) are then modified accordingly. The parameters α_μ and α_ε are subject to the restrictions $\alpha_\mu < 1$ and $\alpha_\varepsilon > -1$ since both μ and ε are positive. Additionally, since the permittivity of all materials is greater than the vacuum permittivity ε_0, we must have $\varepsilon_a(1 + \alpha_\varepsilon) > \varepsilon_0$ for each $\alpha_\varepsilon > -1$. Note that negative values of α_μ and α_ε reverse the direction of bending, as is illustrated in Section 4.

The integral in (2.15) can now be evaluated to give

$$V = \frac{AD_{\mathrm{L}}}{\varepsilon_a[(1 + \alpha_\varepsilon)\lambda_a^2 - \lambda_b^2]} \log\left[(1 + \alpha_\varepsilon)\frac{\lambda_a^2}{\lambda_b^2}\right]. \tag{2.27}$$

Equation (2.25) can also be evaluated to give

$$\mu_a \frac{[\lambda_b^2 - (1 - \alpha_\mu)\lambda_a^2]}{\lambda_b^2 - \lambda_a^2} \left[\frac{3}{4}(\lambda_b^4 - \lambda_a^4) - \log\left(\frac{\lambda_b}{\lambda_a}\right) - (\lambda_b^2 - \lambda_a^2) \right]$$

$$- \frac{1}{2}\mu_a\alpha_\mu \left[\lambda_b^4 + \lambda_a^2\lambda_b^2 + \lambda_a^4 - (\lambda_b^2 + \lambda_a^2) - 1 \right] + K(\lambda_b^2 - \lambda_a^2)$$

$$- \frac{1}{2}D_{\mathrm{L}}^2 \frac{\lambda_b^2 - \lambda_a^2}{\varepsilon_a[\lambda_a^2(1 + \alpha_\varepsilon) - \lambda_b^2]} \log\left[(1 + \alpha_\varepsilon)\frac{\lambda_a^2}{\lambda_b^2} \right] - D_{\mathrm{L}}^2 \frac{\alpha_\varepsilon}{\varepsilon_a(1 + \alpha_\varepsilon)} = 0. \quad (2.28)$$

For a given applied voltage V, after D_{L} is substituted into (2.27) and D_{L}^2 and K into (2.28) from (2.23) and (2.24), the resulting equations yield specific forms of the functions f and g in (2.20) and (2.21), which can now in principle be solved simultaneously for λ_a and λ_b. The dependence of the bending angle φ, given by (2.5), on the applied voltage can then be determined. The corresponding radial and circumferential stress components τ_{rr} and $\tau_{\theta\theta}$ can also be determined, from (2.8) with the specializations (2.10) and (2.22). Numerical results for specific values of α_μ and α_ε are provided in the following section.

3   Numerical results

For numerical purposes we work in terms of the dimensionless quantities:

$$\bar{K} = K/\mu_a, \qquad \bar{V} = \sqrt{\varepsilon_a/\mu_a}V/A, \qquad (3.1)$$

and equations (2.20) and (2.21) take the dimensionless forms

$$\bar{V} = \bar{f}(\lambda_a, \lambda_b), \qquad \bar{g}(\lambda_a, \lambda_b) = 0. \qquad (3.2)$$

These are the dimensionless forms of (2.27) and (2.28) after substitution for D_{L} and K, where

$$\bar{f} = \sqrt{\varepsilon_a/\mu_a}f/A, \qquad \bar{g}(\lambda_a, \lambda_b) = g(\lambda_a, \lambda_b)/\mu_a. \qquad (3.3)$$

Thus, $\bar{f}$ and $\bar{g}$ depend only on λ_a, λ_b and the parameters α_μ and α_ε, i.e. they are independent of μ_a and ε_a.

For an initially rectangular FGDE plate with aspect ratio $L/A = 10$, subject to a (dimensionless) voltage $\bar{V} = 0.2$, Figure 2 depicts the resulting bent shape of the plate for a fixed value of the elastic parameter $\alpha_\mu = 0.3$ and four values of electric parameter α_ε. The plate is bent into a complete circle for $\alpha_\varepsilon = 1.521$. Again for $\alpha_\mu = 0.3$ and three values of α_ε, in Figure 3 the distributions of the radial and circumferential stress components through the plate are shown in dimensionless forms $\bar{\tau}_{rr} = \tau_{rr}/\mu_a$, $\bar{\tau}_{\theta\theta} = \tau_{\theta\theta}/\mu_a$ versus the radial coordinate in the form $\bar{r} = (r - r_a)/(r_b - r_a)$.

As expected intuitively, we find that increasing α_ε makes the plate more susceptible to bending. The stress components vary continuously through the thickness, with the circumferential stress two orders of magnitude larger than that of the radial stress. Interestingly, at least for examples considered here, the bent sector has two neutral surfaces (where
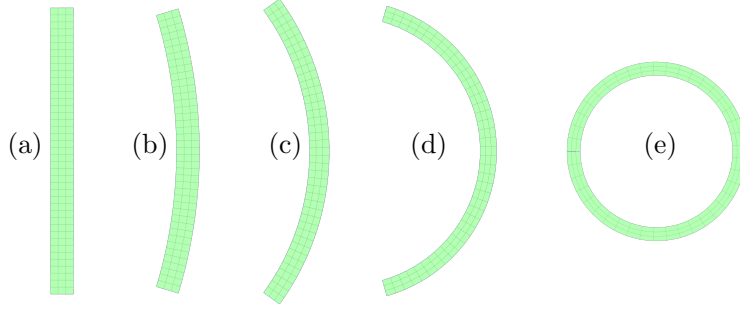
Figure 2: (a) Undeformed rectangular plate cross section with aspect ratio $L/A = 10$. (b)–(e) plate bent by application of a dimensionless voltage $\bar{V} = 0.2$ with the following values of $(\alpha_\varepsilon, \alpha_\mu)$: (b) $(0.3, 0.3)$; (c) $(0.7, 0.3)$; (d) $(1.1, 0.3)$; (e) $(1.521, 0.3)$.
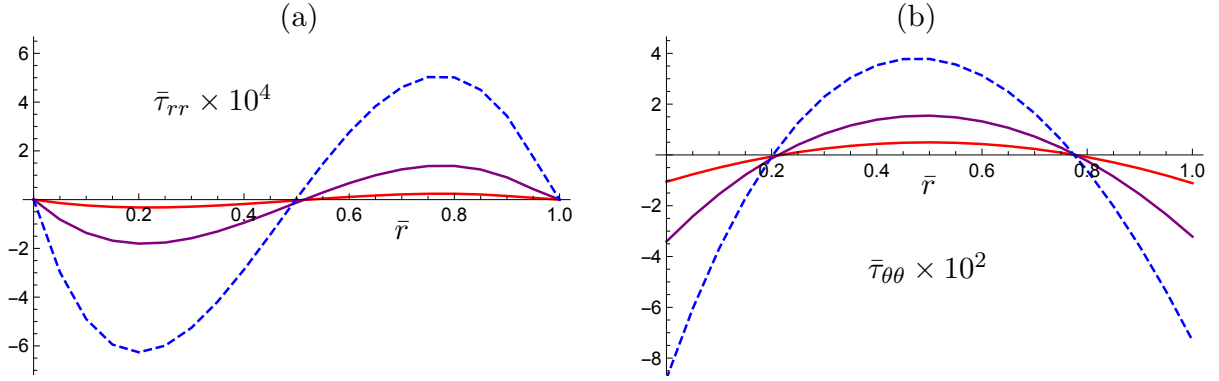

Figure 3: Plots of (a) the radial stress τ_{rr} and (b) the circumferential stress $\tau_{\theta\theta}$ in scaled dimensionless form versus the normalized radius $\bar{r}$ for the dimensionless voltage $\bar{V} = 0.2$ and the following values of $(\alpha_\varepsilon, \alpha_\mu)$: red $(0.1, 0.3)$; purple $(0.4, 0.3)$; blue dashed $(0.7, 0.3)$.

$\tau_{\theta\theta} = 0$). Additionally we note that while on both its inner and outer faces the circumferential stress is *compressive*, these faces are nonetheless in *extension* as the circumferential stretches are greater than 1 there. Similar phenomena were observed for the bending of purely elastic layered plates [11] and swelling functionally graded hydrogel plates [26].

For a fixed value of the electric parameter $\alpha_\varepsilon = 0.4$ and three values of the elastic parameter α_μ, results analogous to those in Figures 2 and 3 are shown in Figures 4 and 5, respectively (now with $\bar{V} = 0.25$). In general, whether bending is enhanced or retarded by a change in α_μ depends on the value of α_ε.

As is clear from the larger value of $\bar{V}$ in Figure 4, as the magnitude of the voltage increases the circular sector becomes more and more bent. As the voltage increases further the sector will eventually form a *complete circular ring*, which, for the values $\alpha_\varepsilon = 0.4, \alpha_\mu = 0.4$, occurs when $\bar{V}$ reaches the approximate value 0.4385. At this point the voltage, however, has not reached its maximum value. Figure 6 shows plots of $\bar{V}$ versus λ_b for different values of α_ε and α_μ, with the points at which a complete circular ring is formed
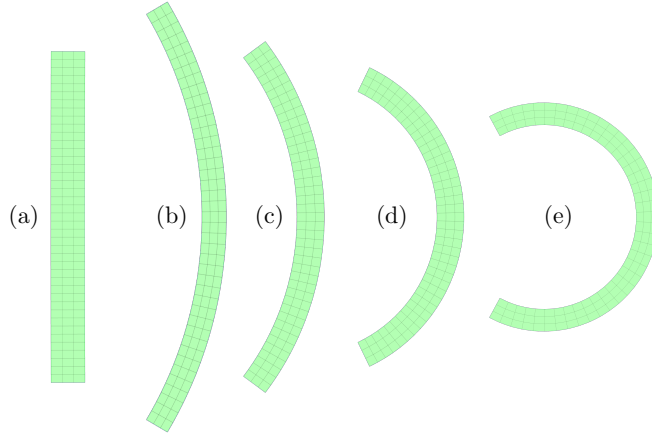
Figure 4: (a) Undeformed rectangular plate cross section with aspect ratio $L/A = 10$. (b)–(d) plate bent by application of a dimensionless voltage $\bar{V} = 0.25$ with the following values of $(\alpha_\varepsilon, \alpha_\mu)$: (b) $(0.4, 0.2)$; (c) $(0.4, 0.4)$; (d) $(0.4, 0.6)$, and (e) with $\bar{V} = 0.4$ and $\alpha_\varepsilon = 0.4, \alpha_\mu = 0.4$.
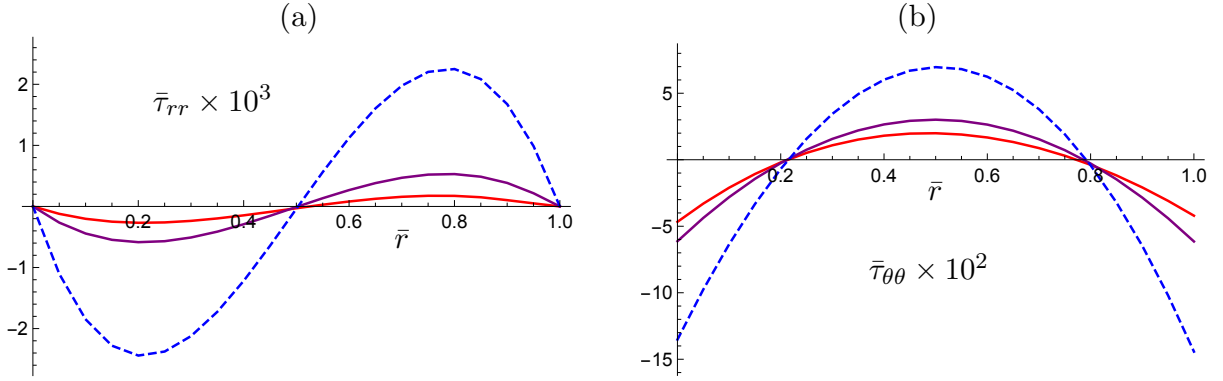

Figure 5: Plots of (a) the radial stress τ_{rr} and (b) the circumferential stress $\tau_{\theta\theta}$ in scaled dimensionless form versus the normalized radius $\bar{r}$ for the dimensionless voltage $\bar{V} = 0.25$ and the following values of $(\alpha_\varepsilon, \alpha_\mu)$: red $(0.4, 0.2)$; purple $(0.4, 0.4)$; blue dashed $(0.4, 0.6)$.

identified by circles, while the crosses mark the (non-accessible) points at which $\bar{V}$ reaches a maximum.

As noted above, it is also seen from Figures 3 and 5 that the inner and outer faces of the bent sector are subject to compressive stress ($\tau_{\theta\theta} < 0$) during the bending deformation for the lower values $\bar{V} = 0.2, 0.25$ before the complete ring forms.

It is of interest to examine at what point the voltage does indeed reach its maximum, and for this purpose V is considered to be a function of λ_b as the independent variable after elimination of K and D_{L}. Then,

$$\frac{\mathrm{d}V}{\mathrm{d}\lambda_b} = \left(\frac{\partial f}{\partial \lambda_b} \frac{\partial g}{\partial \lambda_a} - \frac{\partial f}{\partial \lambda_a} \frac{\partial g}{\partial \lambda_b} \right) \bigg/ \frac{\partial g}{\partial \lambda_a}, \tag{3.4}$$
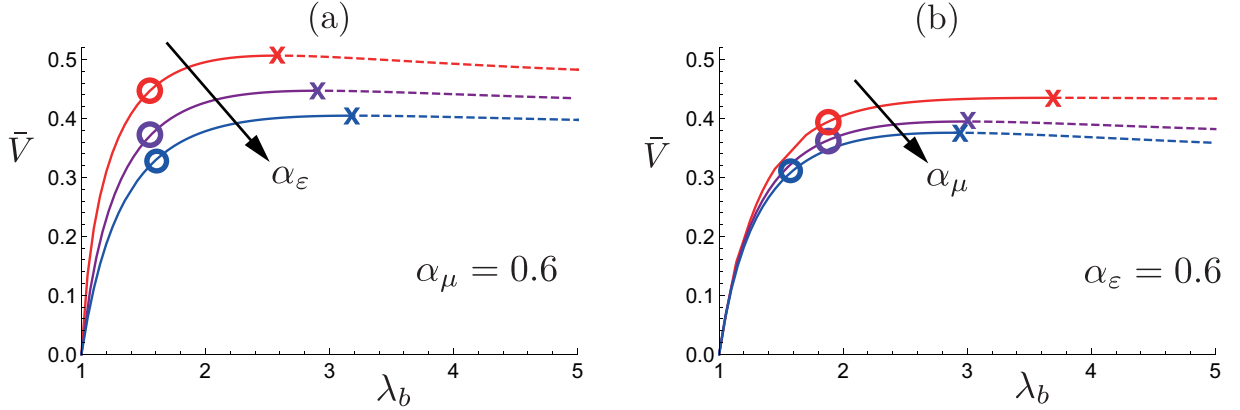
10

Figure 6: Plots of the voltage $\bar{V}$ versus the outer side circumferential stretch λ_b. (a) Plates with elastic parameter $\alpha_\mu = 0.6$ and increasing $\alpha_\varepsilon = 0.1, 0.4, 0.7$, red, purple and blue, respectively; (b) plates with $\alpha_\varepsilon = 0.6$ and increasing elastic parameter $\alpha_\mu = 0.4, 0.5, 0.8$, red, purple and blue, respectively. The circles correspond to points at which a complete circular ring is formed. The maxima of $\bar{V}$, marked with crosses, are beyond these points and are thus never attained.

so that a maximum arises when

$$\det \begin{bmatrix} \dfrac{\partial f}{\partial \lambda_a} & \dfrac{\partial f}{\partial \lambda_b} \\ \dfrac{\partial g}{\partial \lambda_a} & \dfrac{\partial g}{\partial \lambda_b} \end{bmatrix} = 0 \tag{3.5}$$

has nontrivial solutions.

However, because the maximum of V does not occur before the plate is bent into a full circle, it is necessary to examine when instability might arise, which, for example, might occur for given values of the parameters α_μ and α_ε as the voltage increases. This is examined in the next section, based on an energy approach.

As the maximum of V does not occur in the relevant range of deformations we emphasise that, in contrast to what happens when a homogeneous dielectric plate, equi-biaxially deformed under an applied voltage, *the phenomenon of pull-in instability does not appear for a functionally graded plate* under plane strain. We recall that in the homogeneous plane strain expansion of a neo-Hookean dielectric plate, there is also no pull-in instability, because then $\bar{V} = \sqrt{1 - \lambda^{-4}}$, which is a monotone function of the stretch [22]. Here our bending deformation (2.1) is also a plane strain deformation, but the $\bar{V} - \lambda_b$ relationship is not monotone.

Because of the dependence of μ and ε on X_1 there is a lack of symmetry with respect to $X_1 = 0$ and $X_1 = A$. Thus, bearing in mind the limitations on the values of α_μ and α_ε mentioned in Section 2.2, it is possible to consider negative values of α_μ and/or α_ε. This is illustrated in Figure 7 for the fixed value $\alpha_\mu = 0.3$ and four negative values of α_ε with $\bar{V} = 0.3$. The bent configurations in this case are generally thinner and longer than those in Figures 2 and 4.
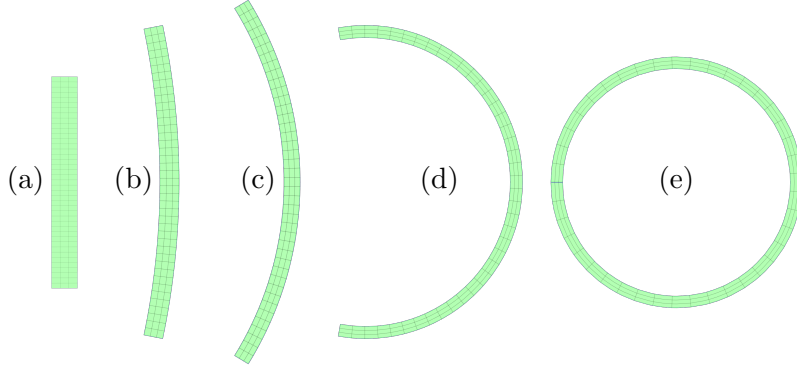
11

Figure 7: (a) Undeformed rectangular plate cross section with aspect ratio $L/A = 10$ and $\bar{V} = 0.3$, with parameters $(\alpha_\varepsilon, \alpha_\mu)$: (b) $(-0.3, 0.3)$; (c) $(-0.45, 0.3)$; (d) $(-0.6, 0.3)$; (e) $(-0.6511, 0.3)$.

Figure 8 illustrates the corresponding radial and circumferential stress distributions, which are quite different from those for the situation with both α_μ and α_ε positive in that the signs of the stresses are the opposite of those in Figures 3 and 5.
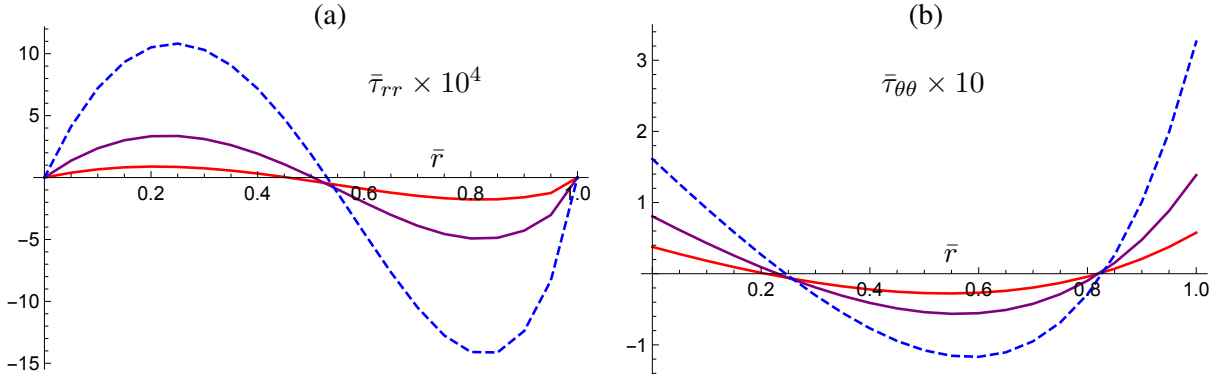

Figure 8: Plots of (a) the radial stress τ_{rr} and (b) the circumferential stress $\tau_{\theta\theta}$ in scaled dimensionless form versus the normalized radius $\bar{r}$ for the dimensionless voltage $\bar{V} = 0.3$ and the following values of $(\alpha_\varepsilon, \alpha_\mu)$: red $(-0.3, 0.3)$; purple $(-0.4, 0.3)$; blue dashed $(-0.5, 0.3)$.

In Figure 9, for fixed parameter values $\alpha_\varepsilon = -0.3, \alpha_\mu = 0.3$, the deformation of a plate with increasing voltage is depicted. The plate thins significantly as it bends further, and no maximum of $\bar{V}$ occurs; the voltage increases monotonically with increasing values of λ_a and λ_b, which are both larger than 1.

A plot of $\bar{V}$ versus λ_b is shown in Figure 10. When $\bar{V}$ reaches the approximate value 0.756 the plate has deformed into a complete circle. The red bullet points identify the values $0.5, 0.6, 0.7, 0.756$ of $\bar{V}$ on the curve corresponding to the bent sectors in Figure 9.

In Figure 11, for fixed values $\alpha_\varepsilon = -0.3, \alpha_\mu = -0.3$, by contrast, as the voltage increases
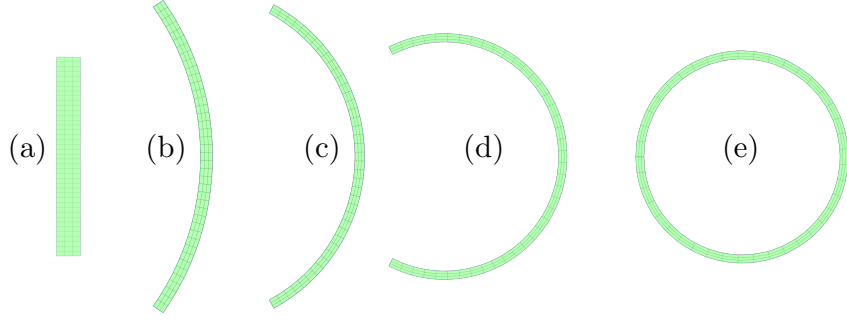
Figure 9: (a) Undeformed rectangular plate cross section with aspect ratio $L/A = 10$ and parameters $\alpha_\varepsilon = -0.3, \alpha_\mu = 0.3$ and the following values of $\bar{V}$: (b) 0.5; (c) 0.6; (d) 0.7; (e) 0.756.
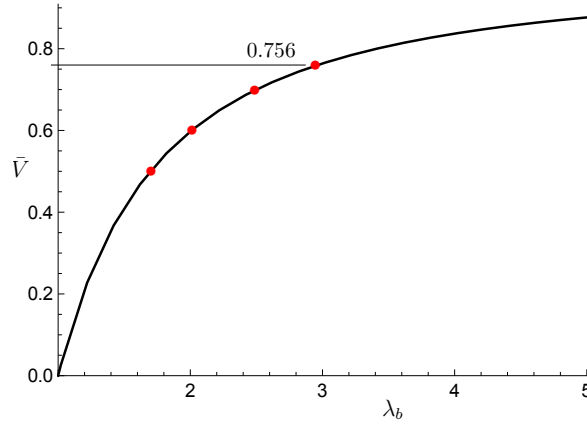

Figure 10: Plot of $\bar{V}$ versus λ_b for the parameters $\alpha_\varepsilon = -0.3, \alpha_\mu = 0.3$ and aspect ratio $L/A = 10$. The red bullet points are associated with the values $0.5, 0.6, 0.7, 0.756$ of $\bar{V}$ in Figure 9(b)–(e), respectively.

the plate bends increasingly to the right until the voltage reaches the approximate value 0.5353, at which point a complete circular ring is formed. Note that the shapes in Figures 2, 4, 7, 9, 11 are not drawn exactly to the correct scale, as the areas should all be the same.

Figure 12 provides the corresponding plot of $\bar{V}$ versus λ_b, with the red bullet points identifying the values $0.3, 0.4, 0.5, 0.5353$ of $\bar{V}$ on the curve corresponding to the bent sectors in Figure 11. In this case the voltage has a maximum, but it is beyond the value at which the complete ring is formed.
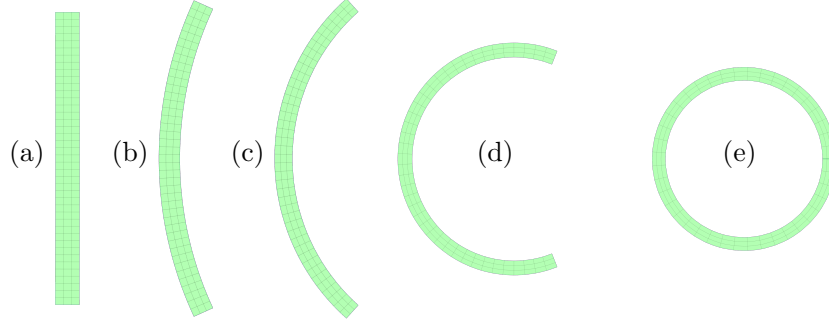
13

Figure 11: (a) Undeformed rectangular plate cross section with aspect ratio $L/A = 10$ and parameters $\alpha_\varepsilon = -0.3, \alpha_\mu = -0.3$ and the following values of $\bar{V}$: (b) 0.3; (c) 0.4; (d) 0.5; (e) 0.5353.
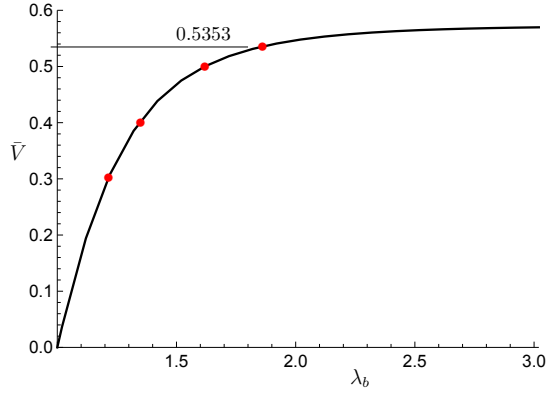

Figure 12: Plot of $\bar{V}$ versus λ_b for the parameters $\alpha_\varepsilon = -0.3, \alpha_\mu = -0.3$ and aspect ratio $L/A = 10$. The red bullet points are associated with the values $0.3, 0.4, 0.5, 0.5353$ of $\bar{V}$ in Figure 11(b)–(e), respectively.

4 Stability analysis

Consider the energy function $\omega^*(\lambda, D_\mathrm{L})$ given by (2.10) with the specialization (2.22) for the considered plane strain situation. We denote by $\omega(\lambda, E_\mathrm{L})$ the corresponding function with the independent variable E_L, related to ω^* by $\omega^*(\lambda, D_\mathrm{L}) = \omega(\lambda, E_\mathrm{L}) + D_\mathrm{L} E_\mathrm{L}$.

From the analysis of Conroy Broderick et al. [28], the *second variation of the free energy density* of a homogeneously deformed plate can be written in terms of either ω^* or ω as

$$\omega^*_{\lambda\lambda}(\delta\lambda)^2 + 2\omega^*_{\lambda D_\mathrm{L}}\delta\lambda\delta D_\mathrm{L} + \omega^*_{D_\mathrm{L} D_\mathrm{L}}(\delta D_\mathrm{L})^2 = \omega_{\lambda\lambda}(\delta\lambda)^2 - \omega_{E_\mathrm{L} E_\mathrm{L}}(\delta E_\mathrm{L})^2, \qquad (4.1)$$

where $\delta\lambda$, δD_L and δE_L, respectively, are variations in λ, D_L and E_L, the corresponding subscripts representing partial derivatives. For the inhomogeneous deformation considered here, this is also the local form of the second variation, and its global counterpart, which

14

requires integration over $X_1 \in [0, A]$ and $X_2 \in [-L/2, L/2]$, is, in terms of ω,

$$L \int_0^A [\omega_{\lambda\lambda}(\delta\lambda)^2 - \omega_{E_L E_L}(\delta E_L)^2] \mathrm{d}X_1 = \frac{2AL}{\lambda_b^2 - \lambda_a^2} \int_{\lambda_a}^{\lambda_b} [\omega_{\lambda\lambda}(\delta\lambda)^2 - \omega_{E_L E_L}(\delta E_L)^2] \lambda \mathrm{d}\lambda. \quad (4.2)$$

We focus initially on the local form of the second variation (4.1). The Hessian matrix associated with the left-hand side of (4.1), denoted $\mathbf{H}^*$, is given by

$$\mathbf{H}^* = \begin{bmatrix} \omega_{\lambda\lambda}^* & \omega_{\lambda D_L}^* \\ \omega_{\lambda D_L}^* & \omega_{D_L D_L}^* \end{bmatrix}. \quad (4.3)$$

It has determinant

$$\det \mathbf{H}^* = \omega_{\lambda\lambda}^* \omega_{D_L D_L}^* - (\omega_{\lambda D_L}^*)^2, \quad (4.4)$$

which can also be written $\omega_{\lambda\lambda} \omega_{D_L D_L}^*$, as shown in Dorfmann and Ogden [27] and Conroy Broderick et al. [28].

For the quadratic form in (4.1) to be strictly positive, $\mathbf{H}^*$ must be positive definite, so that

$$\omega_{\lambda\lambda}^* > 0, \qquad \det \mathbf{H}^* \equiv \omega_{\lambda\lambda} \omega_{D_L D_L}^* > 0. \quad (4.5)$$

For the models

$$\omega^*(\lambda, D_L) = W(\lambda) + \frac{1}{2}\varepsilon^{-1}\lambda^{-2}D_L^2, \qquad \omega(\lambda, E_L) = W(\lambda) - \frac{1}{2}\varepsilon\lambda^2 E_L^2, \quad (4.6)$$

with W given by (2.22), we have

$$\omega_{D_L D_L}^* = \varepsilon^{-1}\lambda^{-2}, \qquad \omega_{E_L E_L} = -\varepsilon\lambda^2. \quad (4.7)$$

Thus, for $\mathbf{H}^*$ to be positive definite, we require

$$\omega_{\lambda\lambda}^* > 0, \qquad \omega_{\lambda\lambda} > 0, \quad (4.8)$$

and, in view of $(4.7)_2$, the global form of the second variation (4.2) is positive if $\omega_{\lambda\lambda} > 0$ for each point of the domain of the integral.

For the models (4.6) with (2.22) the inequalities (4.8) simplify to

$$\mu(1 + 3\lambda^{-4}) + 3\lambda^{-4}\varepsilon^{-1}D_L^2 > 0, \qquad \mu(1 + 3\lambda^{-4}) - \varepsilon E_L^2 > 0. \quad (4.9)$$

The first of these is always satisfied, while the second is

$$\mu(1 + 3\lambda^{-4}) - \lambda^{-4}\varepsilon^{-1}D_L^2 > 0, \quad (4.10)$$

which can be written in terms of the voltage on use of (2.27).

When $\alpha_\mu = \alpha_\varepsilon = 0$ and the deformation is homogeneous, we have

$$\mu^{-1}\lambda^4 \omega_{\lambda\lambda}^* = \lambda^4 + 3 + 3\bar{D}_L^2, \qquad \mu^{-1}\varepsilon\lambda^6 \det \mathbf{H}^* = \lambda^4 + 3 - \bar{D}_L^2 = \mu^{-1}\lambda^4 \omega_{\lambda\lambda}, \quad (4.11)$$

where $\bar{D}_\mathrm{L} = D_\mathrm{L}/\sqrt{\mu_a \varepsilon_a}$, and we also note that $\bar{D}_\mathrm{L} = \lambda^2 \bar{E}_\mathrm{L}$, where $\bar{E}_\mathrm{L} = E_\mathrm{L}\sqrt{\varepsilon_a/\mu_a}$. Then, it is clear that $\omega^*_{\lambda\lambda} > 0$, while $\det \mathbf{H}^*$ can become negative as D_L increases from zero, in which case stability according to the Hessian criterion is lost. Since there is no applied load $\bar{D}^2_\mathrm{L} = \lambda^4 - 1$ and $\bar{E}^2_\mathrm{L} = 1 - \lambda^{-4}$ so that $\bar{D}_\mathrm{L}$ increases indefinitely with λ while $\bar{E}_\mathrm{L}$ increases up to an upper limit 1, i.e. a homogeneous plate in plane strain can only support a maximum non-dimensional voltage $\bar{V} = \bar{E}_\mathrm{L} = 1$. This is different from the equi-biaxial situation where $\bar{E}^2_\mathrm{L}$ exhibits a maximum and pull-in instability occurs; see, for example, [17, 21, 27].

By contrast with (4.11) the inhomogeneity of μ and ε must be accounted for in (4.10). Figure 13 illustrates the results of calculation of $\omega_{\lambda\lambda}$ in terms of dimensionless $\bar{\omega} = \omega/\mu_a$ with $\bar{\omega}_{\lambda\lambda}$ plotted against λ for the relevant range of values of λ_a and λ_b, which is different for each value of the dimensionless voltage $\bar{V}$. The (black) right-most curve in each case corresponds to the value of the voltage at which a complete circular ring is formed. Up to this point in each case $\omega_{\lambda\lambda} > 0$ for each $\lambda \in [\lambda_a, \lambda_b]$, but its value decreases with the voltage. Thus, each configuration is stable according to the Hessian criterion, and the second variation (4.2) is therefore positive. These results apply for the two considered pairs of values of $(\alpha_\varepsilon, \alpha_\mu)$, but we have found similar results for a range of other combinations of these parameters. In view of the local result there is no need to consider the global counterpart (4.2) for the model in question.
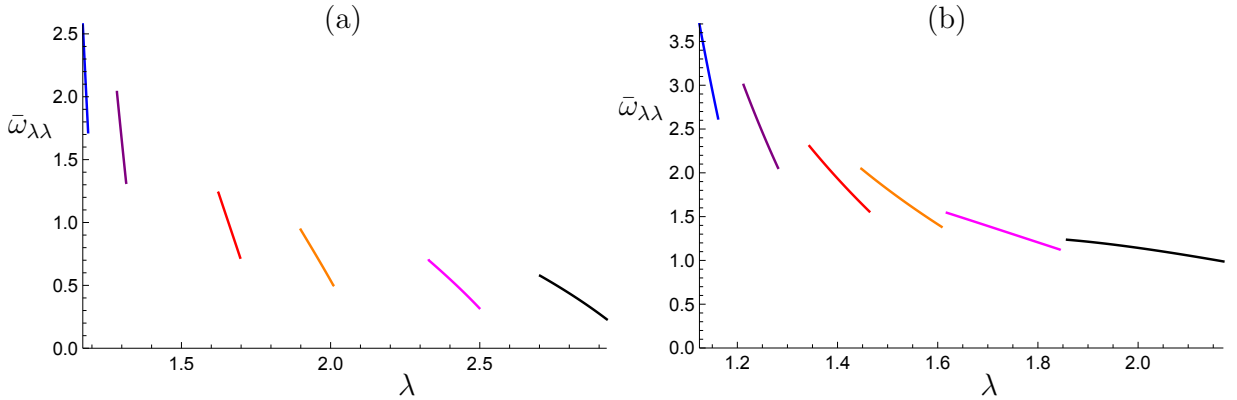

Figure 13: Plots of $\bar{\omega}_{\lambda\lambda}$ versus λ for $\lambda \in [\lambda_a, \lambda_b]$ for each separate value of $\bar{V}$. (a) for $\alpha_\varepsilon = -0.3, \alpha_\mu = 0.3$ with, from left to right, $\bar{V} = 0.2, 0.3, 0.5, 0.6, 0.7, 0.756$. (b) for $\alpha_\varepsilon = -0.3, \alpha_\mu = -0.3$ with, from left to right, $\bar{V} = 0.2, 0.3, 0.4, 0.45, 0.75, 0.5353$.

5   Concluding remarks

In summary, we have investigated the voltage-induced bending response of an FGDE plate, and formulated a method for analyzing its stability based on the positive definiteness of the Hessian.

We found that the 'bendability' of the plate can be tuned by carefully selecting the grading properties, as illustrated here for linear gradients, by choosing appropriate values of the inhomogeneity gradients α_μ and α_ε. A bent sector is subject to compressive circumferential stresses at both its inner and outer surfaces, with two neutral axes.

On analysing the stability we found that the bent configurations are always stable according to the Hessian criterion up to the point that a complete circular ring is formed, the voltage at this point depending on the inhomogeneity parameters α_ε and α_μ.

In contrast with the situation for a homogeneous plate subject to equi-biaxial deformations, where pull-in instability occurs, in the present plane strain problem there in no such pull-in instability. In particular, even though the voltage-stretch curve may exhibit a maximum, it cannot be associated with pull-in instability within the stable domain since a complete ring is formed before the maximum is reached. The analysis herein is based on a particular (neo-Hookean based) constitutive model and a simple form of the material grading properties. It can be expected that the results will be somewhat different, at least quantitatively, for different model choices, but the framework presented here can accommodate more general models.

In this paper we have focused only on the possibility of instability arising from the loss of positive definiteness of the Hessian but we have found that such instability does not arise for the considered model. However, this approach to the analysis of instability tells only part of the story since it does not allow for wrinkling types of instability in membranes [20] or inhomogeneous wrinkling deformations [24, 27], which can be induced [30] by the negative circumferential stress in the elastomer (Figures 3, 5, 8).

Applications where gradient properties could be beneficial are in the design of sensors and actuators and complicated motions of soft robots, for example.

Acknowledgments

References

[1] R. Pelrine, R. Kornbluh, Q. Pei, J. Joseph, High-speed electrically actuated elastomers with strain greater than 100%, Science 287 (2000), 836–839.

[2] A. O'Halloran, F. O'Malley, P. McHugh, A review on dielectric elastomer actuators, technology, applications, and challenges J. Appl. Phys. 104 (2008), 071101.

[3] P. Brochu, Q. Pei, Q, Advances in dielectric elastomers for actuators and artificial muscles, Macromol. Rapid Comm. 31 (2010), 10–36.

[4] I. Alessandri, J. Lombardi, Enhanced Raman scattering with dielectrics, Chem. Rev. 116 (2016), 14921–14981.

[5] B. Nketia-Yawson, Y. Noh, Recent Progress on High-Capacitance Polymer Gate Dielectrics for Flexible Low-Voltage Transistors, Adv. Funct. Mater. 28 (2018), 1802201.

[6] T. Li, G. Li, Y. Liang, T. Cheng, J. Dai, X. Yang, B. Liu, Z. Zeng, Z. Huang, Y. Luo, T. Xie, W. Yang, Fast-moving soft electronic fish Sci. Adv. 3 (2017), e1602045.

[7] T. Li, Z. Zou, G. Mao, X. Yang, Y. Liang, C. Li, S. Qu, W. Yang, Agile and resilient insect-scale robot, Soft Robot 6 (2018), 133–141.

[8] L. He, J. Lou, J. Du, J. Wang, Finite bending of a dielectric elastomer actuator and pre-stretch effects, Int. J. Mech. Sci. 122 (2017), 120–128.

[9] Y. Su, B. Wu, W. Chen, M. Destrade, Pattern evolution in bending dielectric-elastomeric bilayers, J. Mech. Phys. Solids 136 (2020), 103670.

[10] T. Morimoto, F. Ashida, Temperature-responsive bending of a bilayer gel Int. J. Solids Struct. 56 (2015), 20–28.

[11] S. Roccabianca, M.Gei, D. Bigoni, Plane strain bifurcations of elastic layered structures subject to finite bending: Theory versus experiments, IMA J. Appl. Math. 75 (2010), 525–548.

[12] G.E. Knoppers, J.W. Gunnink, J. Van Den Hout, W. Van Vliet, The reality of functionally graded material products, In Intelligent Production Machines and Systems: First I* PROMS Virtual Conference, Elsevier, Amsterdam (pp. 467-474) (2005).

[13] R.M. Mahamood, E.T. Akinlabi, M. Shukla, S. Pityana, Functionally graded material: an overview, Proceedings of the World Congress on Engineering 2012 Vol III, London, UK, (2012).

[14] X. Wang, M. Jiang, Z. Zhou, J. Gou, D. Hui, 3D printing of polymer matrix composites: A review and prospective, Compos. Part B Eng. 110 (2017) 442-458.

[15] A. Dorfmann, R.W. Ogden, Nonlinear electroelastic deformations, J. Elasticity 82 (2006), 99–127.

[16] L. Dorfmann, R.W. Ogden, *Nonlinear Theory of Electroelastic and Magnetoelastic Interactions.* Springer, 2014.

[17] X. Zhao, Z. Suo, Method to analyze electromechanical stability of dielectric elastomers, Appl. Phys. Lett. 91 (2007), 061921.

[18] T. Lu, J. Huang, C. Jordi, G. Kovacs, R. Huang, D. Clarke, Z. Suo, Dielectric elastomer actuators under equal-biaxial forces, uniaxial forces, and uniaxial constraint of stiff fibers, Soft Matter, 8 (2012), 6167–6173.

[19] X. Zhao Q. Wang, Harnessing large deformation and instabilities of soft dielectrics: Theory, experiment, and application. Appl. Phys. Rev. 1 (2014), 021304.

[20] G. Zurlo, M. Destrade, D. DeTommasi, G. Puglisi, Catastrophic thinning of dielectric elastomers. Phys. Rev. Lett. 118 (2017), 078001.

[21] Y. Su, B. Wu, W. Chen, C. Lu, Optimizing parameters to achieve giant deformation of an incompressible dielectric elastomeric plate, Extreme Mech. Lett. 22 (2018), 60–68.

[22] Y. Su, W. Chen, M. Destrade, Tuning the pull-in instability of soft dielectric elastomers through loading protocols, Int. J. Non-Lin. Mech. 113 (2019), 62–66.

[23] R. S. Rivlin, Large elastic deformations of isotropic materials V: the problem of flexure, Proc. Roy. Soc. Lond. Ser. A 195 (1949), 463–473.

[24] Y. Su, B. Wu, W. Chen, M. Destrade, Finite bending and pattern evolution of the associated instability for a dielectric elastomer slab, Int. J Solids Struct. 158 (2019), 191–209.

[25] B. Wu, Y. Su, D. Liu, W. Chen, C. Zhang, On propagation of axisymmetric waves in pressurized functionally graded elastomeric hollow cylinders, J. Sound Vib. 421 (2018), 17–47.

[26] M. Bayat, A. Kargar-Estahbanaty, M. Baghani, A semi-analytical solution for finite bending of a functionally graded hydrogel strip, Acta Mech. 230 (2019), 2625–2367.

[27] L. Dorfmann, R.W. Ogden, Instabilities of soft dielectrics. Phil. Trans. R. Soc. A 377 (2019), 20180077.

[28] H. Conroy Broderick, M. Righi, M. Destrade, R.W. Ogden, Stability analysis of charge-controlled soft dielectric plates. Int. J. Eng. Sci. 151 (2020), 103280.

[29] K. Bertoldi, M. Gei, Instabilities in multilayered soft dielectrics. J. Mech. Phys. Solids 59(1) (2011), 18-42.

[30] G. Mao, Y. Xiang, X. Huang, W. Hong, T. Lu, S. Qu, Viscoelastic effect on the wrinkling of an inflated dielectric-elastomer balloon, J. Appl. Mech. 85(7) (2018).